Ti off-center displacements and the oxygen isotope-induced phase transition in $SrTiO_3$

Y. Yacoby* and Y. Girshberg
Racah Institute of Physics, Hebrew University, Jerusalem 91904, Israel
(Received 27 September 2007; published 29 February 2008)

$SrTiO_3$ (STO) displays a huge isotope effect. Replacing ^{16}O with ^{18}O changes the incipient ferroelectric crystal into a ferroelectric crystal with a transition temperature of 24.5 K. We present a model that takes into account the soft mode, the NMR observed spontaneous Ti off-center displacements present in both $ST^{16}O$ and $ST^{18}O$, and their interaction with each other. Replacing ^{16}O with ^{18}O increases the TiO_3 reduced mass by 5.5%. This is the only effect taken into account, and it affects only the soft mode leaving the Ti off-center displacements and their interaction with the soft mode constant. We show that the model accounts quantitatively for the ferroelectric phase transition, the Raman and neutron scattering observed soft modes, the temperature and ^{18}O concentration dependence of the dielectric constant, and the ^{18}O concentration and pressure dependence of the phase transition temperature.

DOI: 10.1103/PhysRevB.77.064116 PACS number(s): 62.20.D−, 31.30.Gs, 77.80.−e

I. INTRODUCTION

In 1999, Itoh *et al.*[1] discovered that $SrTiO_3$ (STO) has a very large isotope effect. Replacing ^{16}O with ^{18}O induced a ferroelectric (FE) phase transition at about 24.5 K. Various experimental methods have been used to characterize the properties of STO as a function of ^{18}O concentration.[2–7] These measurements showed that the transition temperature T_c as a function of the ^{18}O concentration x seems to obey the relation $T_c(x)=30.4(x-x_c)^{1/2}$, with $x_c=0.33$,[5] and as a function of pressure P, the relation $T_c(P,x=1)=23.9(1-P/P_c)^{1/2}$, with $P_c=0.69$ kbar.[4,7] The nontrivial square root dependence was theoretically predicted for pure displacive like systems in the quantum regime.[8,9]

In pure displacive systems, we expect that the frequency of the soft mode in $SrTi^{16}O_{1-x}{}^{18}O_x$ should soften as ^{18}O concentration increases and should go to zero at T_c. Raman measurements of $ST^{18}O$ (Refs. 10 and 12) found that below T_c, the system has two modes, both polarized perpendicular to the crystal c axis. The modes soften as T_c is approached from below. However, as Shigenari *et al.*[11] pointed out, neither of them goes to zero at T_c. These modes combine to one mode above T_c, and its frequency has been measured by neutron scattering[13] for a number of x values. The frequency of this mode does not go to zero at T_c and is close to that of the mode observed in $ST^{16}O$ in hyper Raman experiments.[15] So, the vibration mode observed in neutron scattering in $SrTi^{16}O_{1-x}{}^{18}O_x$ is the same mode observed in hyper Raman in $ST^{16}O$.

Takesada *et al.*[12] observed another very low frequency mode that comes very close to zero at T_c, suggesting that this is the soft mode that drives the $ST^{18}O$ phase transition. The frequency of this mode is very small, and it is therefore not related to the soft mode observed in hyper-Raman measurements in $ST^{16}O$. Shigenari *et al.*[11] also saw this low frequency mode and referred to it as "quasielastic scattering." Neither group identified the origin of this mode. In conclusion the Raman and neutron data show that above T_c, there are two soft modes, one that remains finite and another that goes to zero at T_c.

The beauty of an isotope effect is that it is very clean. The only change involved is the well known change of the isotope mass. The transverse optic vibration mode that dominates the paraelectric and ferroelectric properties of STO consists mainly of opposite vibrations of the Ti atoms and oxygen octahedra. The reduced mass relevant to this vibration mode is

$$\frac{1}{\mu(x)} \approx \frac{1}{m_{\mathrm{Ti}}} + \frac{1}{3m_{\mathrm{O}}(1+x/8)}, \quad \rho \equiv \frac{\mu(0)}{\mu(x)} = \frac{1+0.0625x}{1+0.125x} \tag{1}$$

where m_{O} is the ^{16}O mass. So, even at $x=1$, $\rho=0.945$; namely, the reduced mass change is less than 6%.

It has been generally assumed that $ST^{16}O$ is a displacive incipient ferroelectric, with its soft mode described reasonably well by the Barrett formula[14]

$$\omega^2 = A\left[\frac{\bar{\omega}}{2}\coth\left(\frac{\bar{\omega}}{2T}\right) - T_0\right]. \tag{2}$$

The parameter values for $ST^{16}O$, as obtained by fitting to Vogt's lower branch,[15] are $A=55.9$ K, $\bar{\omega}=85$ K, and $T_0=39$ K. A is proportional to the square of the bare phonon frequency and is therefore proportional to ρ, and $\bar{\omega}$ is an average over the soft phonon branch frequency and is therefore approximately proportional to $\sqrt{\rho}$. One can easily see that even when the oxygen is fully replaced by ^{18}O, ω^2 is positive. It is necessary to change the reduced mass by about 50% to achieve the experimentally observed phase transition temperature.

Bussmann-Holder and Bishop[16,17] attempted to understand this isotope effect by using their nonlinear shell model[18,19] and by invoking self-induced intrinsic inhomogeneity. The authors found that adjusting the TiO_3 cluster mass reproduces the ferroelectric phase transition in $ST^{18}O$. However, the mass change needed to achieve this result is 40%. Furthermore, this model predicts that the frequency of the soft mode observed in $ST^{16}O$ should decrease with increasing ^{18}O concentration and should vanish at T_c. This result is not supported by the neutron and Raman experimental results.

Yamada *et al.*[13] suggested a pure order-disorder model. According to their model, the soft mode changes with the

oxygen mass, but its frequency does not vanish at T_c and it does not lead to the FE phase transition. Instead the system has, in addition, spontaneous dipoles present above T_c, and this spinlike system induces the FE phase transition. The authors assume that the oxygen mass change somehow changes the tunneling frequency of the spins so that $ST^{16}O$ remains paraelectric while $ST^{18}O$ undergoes a FE phase transition at approximately 24 K. This model predicts, in agreement with the neutron and Raman experiments, that above T_c the system has two vibrational modes: the soft mode with a finite frequency at T_c and the spin mode with a frequency that vanishes at T_c. However, a calculation of the spin mode frequency using the model and parameters of Yamada *et al.*[13] shows that the spinlike mode frequency grows much faster with temperature (by a factor of more than 6) than the experimental results of Takesada *et al.*[12]

NMR experiments[20] showed that the Ti atoms are displaced to off-center positions even in the paraelectric phase. The fact that such displacements have not been observed in x-ray absorption fine structure experiments[21] means that the displacements are smaller than about 0.05 Å. The Ti off-center displacements do not change with the oxygen mass. So, one cannot expect that these displacements by themselves can explain the isotope effect. Indeed, Blinc *et al.*[20] pointed out that the Ti off-center displacements observed in their NMR measurements as well as the soft mode are involved in the ferroelectric transition of $ST^{18}O$.

We present a model that follows a theoretical approach similar to the one we have used to study bulk perovskite ferroelectrics.[22–25] The model takes into account the soft mode, the Ti off-center displacements treated as spins, the spin-spin interaction, as well as the spin-phonon interaction. The tunneling frequency of the spin subsystem and its interaction with the soft mode are constant, while the soft mode changes with the oxygen mass according to well known rules. It turns out that these small changes of the soft mode frequency lead to a strong decrease of the lower spin-phonon mode frequency and to the phase transition at the critical concentration x_c and to the observed FE transition temperature at $x=1$. This model accounts quantitatively for the properties of $ST^{16}O_{1-x}{}^{18}O_x$.

In Sec. II, we present the theory, followed by a comparison with experimental results in Sec. III. The results are summarized in Sec. IV.

II. THEORY

The system Hamiltonian consists of five parts,[24–26]

$$H = H_{el} + H_{ph} + H_{el\text{-}ph} + H_S + H_{S\text{-}ph}. \tag{3}$$

H_{el} and H_{ph} are the two-band electron and bare transverse polar optical phonon Hamiltonians, respectively,

$$H_{el} + H_{ph} = \sum_{\mathbf{p},\alpha} \epsilon_\alpha(\mathbf{p}) a^+_{\alpha,\mathbf{p}} a_{\alpha,\mathbf{p}} + \sum_{\mathbf{q}} \omega_0(\mathbf{q}) b^+_{\mathbf{q}} b_{\mathbf{q}}. \tag{4}$$

Here, $\alpha=1,2$ for conduction and valence bands, respectively, $\epsilon_\alpha(\mathbf{p})$ is the electronic energy in band α and momentum $\mathbf{p}$, $\omega_0(\mathbf{q})$ is the frequency of the bare phonon with wave vector $\mathbf{q}$, and $a(a^+)$ and $b(b^+)$ are the electron and phonon creation (annihilation) operators, respectively.

The interband electron-transverse phonon interaction is given by

$$H_{el\text{-}ph} = \frac{1}{\sqrt{N}} \sum_{\mathbf{k},\mathbf{p}} \Gamma \sqrt{\frac{\omega_0(\mathbf{k})}{2}} (b_{\mathbf{k}} + b^+_{-\mathbf{k}})(a^+_{1,\mathbf{p}} a_{2,\mathbf{p}-\mathbf{k}} + a^+_{2,\mathbf{p}} a_{1,\mathbf{p}+\mathbf{k}}), \tag{5}$$

where Γ is the coupling constant. Finally, the last two parts are the Ising-like spin-phonon Hamiltonian in a transverse field,

$$H_S + H_{S\text{-}ph} = \sum_{\mathbf{p}} \Upsilon(\mathbf{p}) \sigma^z_{\mathbf{p}} \sigma^z_{-\mathbf{p}} + \sum_i \Omega_0 \sigma^x_i + \frac{1}{\sqrt{N}} \sum_{\mathbf{k}} \frac{f(\mathbf{k})}{\omega_0(\mathbf{k})} \sqrt{\frac{\omega_0(\mathbf{k})}{2}} (b_{\mathbf{k}} + b^+_{-\mathbf{k}}) \sigma^z_{-\mathbf{k}} \tag{6}$$

Here, σ is the Pauli spin matrix, Υ is the direct spin-spin interaction constant, i is the site index, and $f(k)$ is the spin-phonon coupling constant. Ω_0 is the tunneling frequency of individual Ti ions before taking direct spin-spin interaction into account. The importance of the direct spin-spin interaction in this case is further discussed toward the end of this paper. Hamiltonians of this type are well understood and commonly used to describe order-disorder-like phase transitions (the Kobayashi model[27,28]). In our case, however, there is an essential difference: The spins interact with a soft mode, and, as noted in Ref. 24, it leads to a strong temperature dependence of the effective spin-spin coupling constant.

The soft mode frequency after the electron-phonon interaction, but prior to the interaction with the polar spin system, is derived in the Appendix and Refs. 24 and 25, and is given by

$$\omega^2(0) = \omega_0^2 \left[-|\Delta_0| + \frac{3\omega_0^2}{2\bar{E}N} \sum_{\mathbf{p}} \frac{1}{2\omega(\mathbf{p})} \coth\left(\frac{\omega(\mathbf{p})}{2T}\right) \right], \tag{7}$$

where

$$\Delta_0 = 1 - \frac{4\Gamma^2}{\bar{E}}. \tag{8}$$

$\omega_0^2 = \omega_0^2(0)$ and $\bar{E}$ is the average energy gap between the highest valence band and the lowest conduction band. As in other perovskite crystals, $|\Delta_0| \ll 1$. The soft mode frequency depends on the isotope mass. This dependence enters only through the dependence of the bare phonon frequency on the oxygen mass.

The interaction of the soft mode with the spin system leads to two combined spin-phonon modes,

$$\tilde{\omega}^2 = \frac{1}{2} \left[\omega^2(0) + \Omega^2(0) + \sqrt{[\omega^2(0) - \Omega^2(0)]^2 + 4|f(0)|^2 \Omega_0 \tanh\left(\frac{\Omega_0}{T}\right)} \right], \tag{9}$$

$$\tilde{\Omega}^2 = \frac{1}{2}\left[\omega^2(0) + \Omega^2(0) - \sqrt{[\omega^2(0) - \Omega^2(0)]^2 + 4|f(0)|^2\Omega_0 \tanh\left(\frac{\Omega_0}{T}\right)}\right], \tag{10}$$

where

$$\Omega^2(\mathbf{k}) = \Omega_0^2\left(1 - \frac{\Upsilon(\mathbf{k})}{\Omega_0}\right). \tag{11}$$

The system undergoes a ferroelectric phase transition when the lower frequency mode vanishes, $\tilde{\Omega}=0$, namely, when

$$\omega^2(0,x,T_c)\Omega^2(0) = \Omega_0|f(0)|^2 \tanh\left(\frac{\Omega_0}{T_c}\right). \tag{12}$$

This is an implicit equation for $T_c(x)$. The dielectric constant at zero frequency can now be obtained and is equal to

$$\varepsilon = \frac{c}{\tilde{\omega}^2(x,T)\tilde{\Omega}^2(x,T)} = \frac{c_e}{\omega^2(0,x,T)\Omega^2(0) - \Omega_0|f(0)|^2 \tanh\left(\frac{\Omega_0}{T}\right)}. \tag{13}$$

Notice that Eq. (7) is an implicit equation for $\omega^2(0)$. Barrett's formula [Eq. (2)] is an approximation of Eq. (7). Its advantage is that it provides an explicit expression for $\omega^2(\mathbf{k})$. Using Barrett's formula and a proper choice of the parameters results in a very good agreement with the experimental values of the dielectric constant ϵ measured by Müller and Burkard[29] in the temperature regions $T<3$ K and $T>30$ K. However, the fit is not good enough in the region in between. In the present case, this temperature range is particularly important because the FE transition temperatures of $SrTi^{16}O_{1-x}{}^{18}O_x$ happen to be in this range. We have therefore developed, in the Appendix, a better approximation of Eq. (7), which is still implicit but convenient to handle computationally. We assume that close to the Brillouin zone center, $\omega^2(q)=\omega^2(0)+Bq^2$, while further out, $\omega^2(q)=\omega^2(0)+\omega_m^2$. This approximation takes into account the fact that the soft mode softens toward the center of the Brillouin zone and saturates far away from it. The approximation is valid, provided that $\omega^2(0) \ll \omega_m^2$, so it is valid up to $\sim$100 K, but it is not applicable at much higher temperatures. Using the above approximation, we have obtained in the Appendix the soft mode frequency squared at $k=0$. As a result of the isotope effect, the bare frequency squared and the saturation frequency squared are both proportional to $\rho(x)$. So, the soft mode frequency squared as a function of ^{18}O concentration and temperature is given by

$$\omega^2(0) = -a\rho(x) + c_1\rho^2(x)\frac{\coth\left(\frac{\sqrt{\omega^2(0)+\omega_m^2\rho(x)}}{2T}\right)}{\sqrt{\omega^2(0)+\omega_m^2\rho(x)}} + c_2\rho^2(x)\int_0^1 \frac{\coth\left(\frac{\sqrt{\omega^2(0)+\omega_m^2\rho(x)q^2}}{2T}\right)}{\sqrt{\omega^2(0)+\omega_m^2\rho(x)q^2}} q^2 dq, \tag{14}$$

where a, c_1, and c_2 are treated as adjustable parameters to be determined by a comparison with experiment. The relation of these parameters to the basic model parameters are discussed in the Appendix.

It turns out, as discussed further down, that in the temperature range of interest $\Omega_0/T>1.5$. Thus, $\tanh(\Omega_0/T)\approx 1$. So, we can evaluate the model using seven parameters: a, c_1, c_2, c_e, ω_m, $\Omega(0)$, and F, where $F=\Omega_0|f(0)|^2$. None of these parameters depend on the oxygen mass. The first five parameters are determined almost entirely from the properties of $ST^{16}O$, while the last two are adjusted to fit the observed properties of $SrTi^{16}O_{1-x}{}^{18}O_x$. The parameters that gave an overall best agreement with the various experiments discussed below were $a=18\,000$ K^2, $c_2=7.72\times10^6$ K^3, $c_1=1.87\times10^6$ K^3, $c_e=1.72\times10^8$ K^4, $\omega_m=313$ K, $\Omega(0)=6.75$ K, and $F=2650$ K^4. In the Appendix, we compare the values of these parameters with the values that one would expect from known parameters deduced from high temperature measurements. At low temperatures, $SrTiO_3$ is in the antiferrodistortive phase that leads to a splitting of the soft mode. Thus, the fit parameters obtained by fitting to the lower branch are not expected to be equal to parameters obtained from experiments done in the cubic phase. Furthermore, the approximation made in Eq. (14) is not valid at high temperatures. However, we do expect the values to be reasonably comparable.

III. COMPARISON WITH EXPERIMENT

In the following, we compare the theoretically calculated and experimentally measured values of a number of properties of $SrTi^{16}O_{1-x}{}^{18}O_x$. Below the antiferrodistortive phase transition, $ST^{16}O$ is tetragonal, and the soft mode measured by Vogt and displayed in his Fig. 6 (Ref. 15) splits into two branches. The lower branch corresponds to a vibration polarized perpendicular to the tetragonal axis. In our model, we treat only the lowest frequency modes, so this mode corresponds to our upper combined spin-phonon (UCS) mode. (The difference between the UCS and the soft mode in $ST^{16}O$ is very small.) The experimental and theoretically calculated frequencies are shown in Fig. 1 and, as can be seen, are in good agreement with each other. The experimentally measured[29] dielectric constant of $ST^{16}O$ is shown in Fig. 2 as a function of temperature, together with the dielectric constant calculated using Eqs. (14) and (13). As can be seen, the two are in excellent agreement, including the temperature range between 5 and 30 K, where the Barrett equation does not give good results.[29] Fitting these two data sets resulted in the first five parameters. The remaining two parameters have

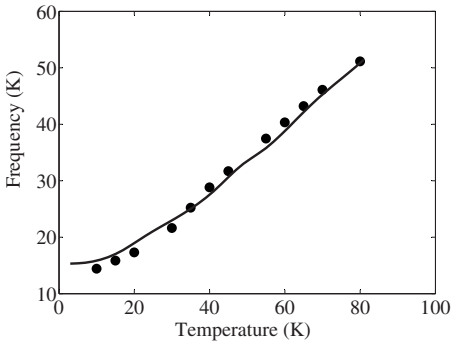

FIG. 1. Comparison of the calculated (solid line) and measured (Ref. 15) (dots) upper combined spin-phonon frequencies as a function of temperature.

a slight influence on the fits. This was taken into account, but the effect on the parameters was small.

The theoretically calculated spin-phonon frequencies in the paraelectric phase of $ST^{18}O$ are shown in Fig. 3. Each branch is expected to split into two below T_c. (We did not calculate the frequencies below T_c because the calculations are much more complicated and require additional parameters.) The measured frequencies below T_c, taken from Fig. 14(a) of Ref. 11, are also shown in Fig. 3. Notice that the two branches are split already at T_c, indicating that the transition is actually first order. Indeed, the theoretically calculated transition temperature calculated from Eq. (12) is $T_{c0}=22.5$ K; namely, it is about 2 K below the measured transition temperature of $T_c=24.5$ K. Notice also that the calculated frequency at T_c is slightly larger than the lower branch but smaller than the upper branch. So, its value is consistent with the measured frequencies below T_c. The phonon frequencies measured by neutron scattering[13] above T_c for $x=0.89$ are also shown in Fig. 3. We interpret this mode to be the upper combined spin-phonon mode. The calculated frequencies are smaller than the measured ones by about 2 K close to T_c growing to about 5 K at 70 K. To the best of our knowledge, the original results have not been published, so it is difficult to assess their accuracy (see Ref. 13).

Of particular interest is the low frequency mode observed by Takesada *et al.*[12] This mode can be clearly seen above T_c in their Fig. 1. This mode has a very small frequency, and it decreases almost to zero at T_c. A similar mode was also observed by Shigenari *et al.*, for example, in their Figs. 8(a)(1) and 8(a)(2).[11] We interpret this mode as the lower spin-phonon combined mode. The experimental and theoretically calculated frequencies of this mode above T_c are shown in Fig. 3 and, as can be seen, are in good agreement with each other.

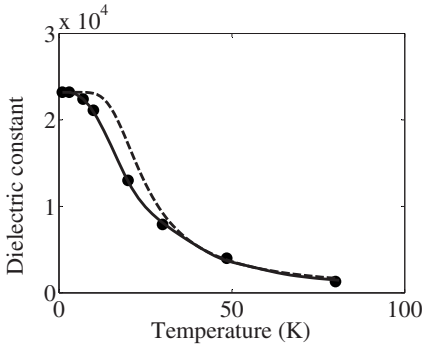

FIG. 2. The dielectric constant of $ST^{16}O$ as a function of temperature. Solid line, calculated using Eqs. (14) and (13); dashed line, calculated using the Barrett formula (Ref. 14); dots, measured (Ref. 29).

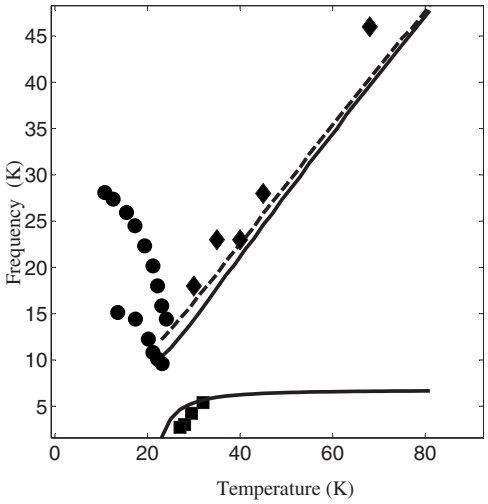

FIG. 3. Phonon frequencies as a function of temperature. Dots, experimentally measured Raman frequencies below T_c taken from Ref. 11; squares, lowest mode frequencies slightly above T_c taken from Ref. 12; diamonds, neutron measurements at $x=0.89$ (Ref. 13); solid lines, the calculated frequencies above T_c of the upper and lower combined spin-phonon modes; dashed line, calculated frequencies of the upper combined spin-phonon mode for $x=0.89$.

Measurements of the dielectric function have been reported in papers by Wang and Itoh.[5] The temperature dependence seems qualitatively reasonable in all samples; however, the size of the dielectric function, for example, at the peak changes in a peculiar way. The peak value of the dielectric constant oscillates with ^{18}O concentration. Consequently, we cannot expect the theoretical and experimental values to be in quantitative agreement. The theoretical and experimental results would also not agree close to T_c because the experimental value is finite while the theoretical one extrapolates to infinity. In spite of these reservations, we tried to compare the two above T_c, and we found that in four of the samples with ^{18}O concentrations of $x=0$, 0.38, 0.6, and 0.84, the theoretical values mimic the experiment quite well with no parameter adjustments. These results are shown in Fig. 4.

The FE transition temperatures as a function of the ^{18}O concentration were measured by Wang and Itoh[5] and are shown in Fig. 5, together with the extrapolated second-order phase transition temperatures determined from Eq. (12). The difference between the experimentally measured first-order transition temperature and the extrapolated second-order transition temperature is about 2 K for large ^{18}O concentrations. This difference decreases at lower ^{18}O concentrations. Taking this difference into account, the agreement between the theory and experiment is excellent.

The dielectric functions of $ST^{16}O$ and $ST^{18}O$ have been measured as a function of hydrostatic pressure. Pressure af-

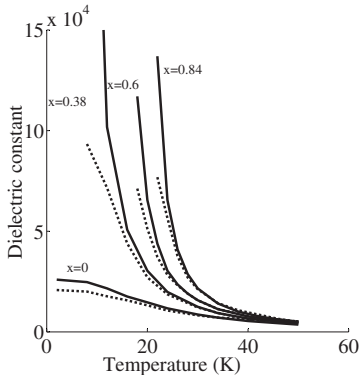

FIG. 4. The dielectric constant as a function of temperature for different ^{18}O concentrations. Dotted line, experiment (Ref. 5); solid line, calculated values.

fects the soft mode frequency of both $ST^{16}O$ and $ST^{18}O$ and the phase transition temperature of $ST^{18}O$. We first compared the dielectric constants of $ST^{16}O$ at 0 bar, measured by Venturini *et al.*[7] and by Müller and Burkard.[29] For the two to agree with each other, it was necessary to decrease the dielectric function of Venturini *et al.*[7] by 500 and to multiply it by a factor of 1.175. These differences in the experimental results are probably due to differences in the experimental setups and in the samples. We then applied these same changes to the dielectric function of $ST^{16}O$ under 0.7 kbar. This is shown in Fig. 6. The term most sensitive to hydrostatic pressure is Δ_0 in Eq. (7) because, as seen in Eq. (8), it is the difference between unity and a term close to unity. Pressure increases the average electronic gap $\bar{E}$, thus decreasing $|\Delta_0|$. This then causes $\omega^2(0)$ to increase pushing the transition temperature down,

$$|\Delta_0(P)| - |\Delta_0| = -\gamma P|\Delta_0| = -\frac{\bar{E}(P) - \bar{E}(0)}{\bar{E}(0)}, \qquad (15)$$

where γ is positive.

We adjusted γ so as to obtain best fit between the theoretical and measured dielectric constants of $ST^{16}O$ as a function of temperature at $P=0.7$ kbar. $\gamma=0.0262$ kbar^{-1}. The results are shown in Fig. 6 and, as can be seen, are in very good agreement with experiment. As shown in the Appendix, the pressure dependence obtained here for $SrTiO_3$ is in good

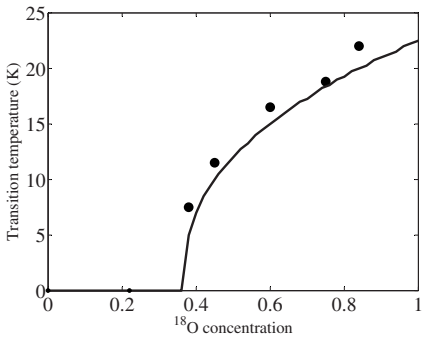

FIG. 5. Measured (Ref. 5) (dots) and calculated (solid line) phase transition temperatures as a function of ^{18}O concentration.

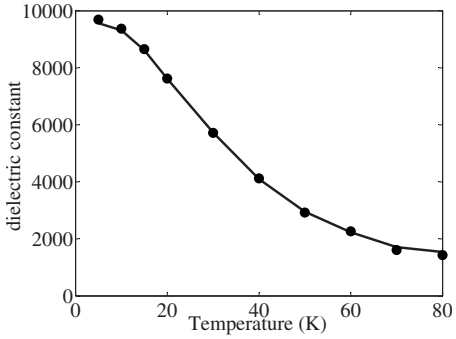

FIG. 6. Dielectric constant of $ST^{16}O$ as a function of temperature at 0.7 kbar pressure. Dots, experiment (Ref. 7); Solid line, calculation.

agreement with the corresponding dependence obtained for $BaTiO_3$ Ref. 30 and $KNbO_3$.[31]

The FE transition temperatures as a function of pressure were taken from Fig. 2 of Venurini *et al.*[7] and are presented here in Fig. 7 together with the calculated values using no additional parameters. Notice that the measured values in Fig. 7 are the first-order transition temperatures, while the calculated ones are the extrapolated second-order transition temperatures. As expected, the difference between the two is 2 K at 0 bar, decreasing to zero at 0.7 kbar. Taking this consideration into account, the theoretical and experimental results for T_c as a function of pressure are also in excellent agreement.

The Ti off-center displacement and their interaction with each other and the soft mode deserve some further discussion. As mentioned in the Introduction, the size of the off-center displacements is smaller than 0.05 Å. If one tries to construct a local potential with a minimum at 0.05 Å away from the center and a reasonable local vibration frequency, say, less than 10^{13} Hz, one finds that the tunneling frequency $\Omega_0 > 100$ K. Thus, in the temperature range of the FE transitions $\Omega_0/T \gg 1.5$. However, the frequency of these polar spins is too high, and their interaction with the soft mode would not give rise to a combined mode that leads to a phase transition. In all the cases we have previously discussed, direct spin-spin interaction was neglected. For example, the FE transition temperature of $PbTiO_3$ and $KNbO_3$ is much higher

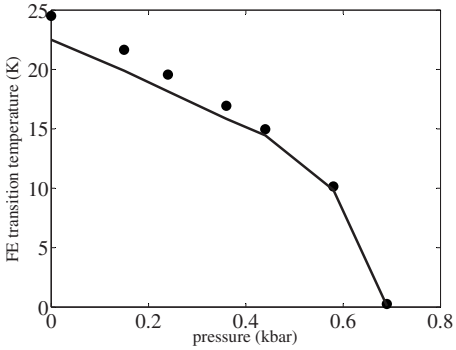

FIG. 7. Ferroelectric transition temperature of $ST^{18}O$ as a function pressure. Dots, experiment (Ref. 7); solid line, calculated values.

than room temperature,[24] so tunneling and direct spin-spin interactions do not play any role. In $KTaO_3$ with Nb,[25] direct spin-spin interaction was negligible because the Nb concentration was small and the Nb ions were far apart. On the other hand, in STO the Ti ions are close to each other and the temperatures of interest are low. So, direct spin-spin interaction does play an important role. It creates a polar spin wave with a zone center frequency of $\Omega(0)=6.75$ K. This frequency is much lower than the tunneling frequency of the individual Ti polar spins, and it is this polar spin wave that interacts with the soft mode and gives rise to the phenomena discussed above.

IV. SUMMARY

The model we have presented here consists of the soft mode of STO and the spontaneous off-center displacements of the Ti atoms. The Ti displacements are treated as polar spins that interact with each other, giving rise to a polar spin wave with a rather low frequency at the Brillouin zone center. This spin wave interacts with the soft mode, creating combined spin-phonon modes. The polar spin system does not change with oxygen mass. Only the soft mode changes strictly according to the change of the TiO_3 reduced mass. The model uses seven adjustable parameters, five of which are essentially determined by properties of $ST^{16}O$. The two additional parameters allow us to account quantitatively for a variety of $SrTi^{16}O_{1-x}{}^{18}O_x$ properties. In addition, we introduce another parameter to account for the pressure dependence of the soft mode of $ST^{16}O$. Using this parameter, we quantitatively account for the pressure dependence of the phase transition temperature of $SrTi^{16}O_{1-x}{}^{18}O_x$. In conclusion, the model accounts for the vibration modes observed in Raman and neutron experiments both the mode that softens but does not vanish at T_c and the mode that vanishes at T_c. Our results agree with the temperature and the ^{18}O concentration dependence of the dielectric constant, and they agree very well with the ^{18}O concentration dependence and pressure dependence of the FE transition temperature.

ACKNOWLEDGMENTS

The authors would like to thank Roy Clarke of the University of Michigan, Ann-Arbor and E. A. Stern of the University of Washington, Seattle for critically reading the manuscript and for their important comments.

APPENDIX: SOFT MODE FREQUENCY

To calculate the soft mode frequency after interband electron-phonon interaction, we use the temperature diagram technique expressing the operators in the Matsubara representation.[32] The renormalized phonon spectrum defined by the Hamiltonian in Eqs. (4) and (5) is given by the poles of the full phonon Green's function $D(\mathbf{k},\Omega_n)$,

$$D(\mathbf{k},\Omega_n) = -\frac{\omega_0^2(\mathbf{k})}{\Omega_n^2+\omega^2(\mathbf{k})}, \tag{A1}$$

where $\Omega_n=2\pi nT$, $n=1,2,3,\ldots$.

D satisfies the Dyson equation, and for the phonon frequencies renormalized by the electron-phonon interaction, we have

$$\omega^2(\mathbf{k}) = \omega_0^2(\mathbf{k})(1+\Pi), \tag{A2}$$

where Π is the total polarization operator of the system.

To all orders of perturbation, the diagrams for the polarization operator contain averages of electron and phonon operators. Since the different types of operators commute with each other, the averages can be calculated separately for operators of different types and can be related to the phonon Green's function [Eq. (A1)] and the electron Green's function,

$$G_{\alpha\alpha}(\mathbf{p},\epsilon_n) = \frac{1}{\imath\epsilon_n - \epsilon_\alpha(\mathbf{p})}. \tag{A3}$$

Here, α is the band index and $\epsilon_n=(2n+1)\pi T$. [$\epsilon(\mathbf{p})$ is measured from the middle of the energy gap E_g, so that the chemical potential $\mu=0$.]

To all orders of perturbation, each diagram consists of an electron loop and a number of internal phonon lines (phonon Green's functions). A diagram of order n contains $(n-1)$ internal phonon lines and is proportional to the interaction parameter Γ^{2n}. So, the first-order diagram is a pure electron loop.

In calculating the diagrams, it is necessary to sum over all internal electron (ϵ_n) and phonon (Ω_n) frequencies. The frequencies of the electronic Green's function that contribute most to the sum lie near to the poles, i.e., $\epsilon_n \geqslant E_g/2$, whereas the corresponding frequencies of the phonon Green's function, $\Omega_n \approx \omega(k)$, are much smaller. Therefore, the temperature summation in the diagrams can be carried out for the electron and phonon Green's functions separately. This is specific to interband electron-phonon interaction. For the same reason, each internal (additional) phonon line introduces an additional small factor, $(T/\bar{E}) \ll 1$, so that the expansion parameter is not the interaction constant $(\Gamma^2/\bar{E})^n \approx 1$, but the parameter $(\Gamma^2/\bar{E})^n(T/\bar{E})^{(n-1)} \ll 1$. This allows us to restrict ourselves to diagrams linear in temperature.

In this approximation, the polarization operator Π contains four diagrams: one first-order diagram (Π_0), "pure" electron loop, and three second-order diagrams with one internal phonon line (Π_1). The diagrams are computed in the usual way.[32]

The first diagram is given by

$$\Pi_0(k) = -\frac{4\Gamma^2}{N}\int \frac{[n(\epsilon_2)-n(\epsilon_1)]d\mathbf{p}}{\epsilon_1(\mathbf{p}+\mathbf{k})-\epsilon_2(\mathbf{p})} = -\frac{4\Gamma^2}{\bar{E}} + bk^2. \tag{A4}$$

Here, $n(\epsilon_\alpha)$ is the Fermi distribution function. Since $T \ll E_{gap}$, $n(\epsilon_1)=0$ and $n(\epsilon_2)=1$, so Π_0 is independent of temperature.

Each one of the Π_1 diagrams contains one phonon line that introduces the temperature dependence and is given by

$$\Pi_1 = \frac{1}{2\bar{E}}\left(\frac{4\Gamma^2}{\bar{E}}\right)^2 \frac{1}{N}\sum_{\mathbf{q}} \frac{\omega_0^2(\mathbf{q})}{2\omega(\mathbf{q})} \coth\left(\frac{\omega(\mathbf{q})}{2T}\right). \tag{A5}$$

In all ferroelectric crystals as well as $SrTiO_3$ (ignoring quantum effects), the paraelectric structure is unstable at $T=0$. Therefore, $4\Gamma^2/\bar{E} > 1$, but since $T_c \ll \bar{E}$, $|\Delta_0| = 4\Gamma^2/\bar{E} - 1 \ll 1$. So, $\omega^2(k)$ is given by

$$\omega^2(\mathbf{k}) = \omega_0^2(\mathbf{k})\left[-|\Delta_0| + bk^2 + \frac{3}{2\bar{E}}\sum_{\mathbf{q}} \frac{\omega_0^2(\mathbf{q})}{2\omega(\mathbf{q})} \coth\left(\frac{\omega(\mathbf{q})}{2T}\right)\right]. \tag{A6}$$

The soft mode dispersion is mainly due to the bk^2 term, so we neglect the bare phonon dispersion, namely, $\omega_0^2(p) = \omega_0^2$. At $k=0$, we obtain Eq. (7).

Equation (7) is an implicit equation for $\omega^2(0)$. In its present form, it is very difficult to solve. We therefore make the following approximations. First, we assume that up to a certain momentum value p_0,

$$\omega^2(p) = \omega^2(0) + Bp^2, \tag{A7}$$

while beyond this value,

$$\omega^2(p) = \omega^2(0) + \omega_m^2 \tag{A8}$$

and

$$\omega_m^2 = Bp_0^2. \tag{A9}$$

Here, $B = \omega_0^2 b$.

We now convert the sum to an integral expression,

$$\omega^2(0) = -\omega_0^2|\Delta_0| + \frac{3\tilde{V}\omega_0^4}{2V_{BZ}\bar{E}} \frac{\coth\left(\frac{\sqrt{\omega^2(0)+\omega_m^2}}{2T}\right)}{2\sqrt{\omega^2(0)+\omega_m^2}} + \frac{12\pi\omega_0^4}{2V_{BZ}\bar{E}}\int_0^{p_0} p^2 dp \frac{\coth\left(\frac{\sqrt{\omega^2(0)+Bp^2}}{2T}\right)}{2\sqrt{\omega^2(0)+Bp^2}}. \tag{A10}$$

Here, V_{BZ} is the volume of the Brillouin zone and $\tilde{V}$ is the volume of the Brillouin zone excluding the volume of a ball with radius p_0.

We can now change the integration variable $p = p_0 q$ and obtain

$$\omega^2(0) = -\omega_0^2|\Delta_0| + \frac{3\tilde{V}\omega_0^4}{2V_{BZ}\bar{E}} \frac{\coth\left(\frac{\sqrt{\omega^2(0)+\omega_m^2}}{2T}\right)}{2\sqrt{\omega^2(0)+\omega_m^2}} + \frac{12\pi\omega_0^4 p_0^3}{2V_{BZ}\bar{E}}\int_0^1 q^2 dq \frac{\coth\left(\frac{\sqrt{\omega^2(0)+\omega_m^2 q^2}}{2T}\right)}{2\sqrt{\omega^2(0)+\omega_m^2 q^2}}. \tag{A11}$$

We now define three parameters that will be determined by comparison with experimental results,

$$a = \omega_0^2|\Delta_0|, \tag{A12}$$

$$c_1 = \frac{3\omega_0^4}{4\bar{E}}\frac{\tilde{V}}{V_{BZ}}, \tag{A13}$$

$$c_2 = 3\frac{3\omega_0^4}{4\bar{E}}\frac{4\pi p_0^3}{3V_{BZ}}. \tag{A14}$$

Notice that $\frac{\tilde{V}}{V_{Bz}} + \frac{4\pi p_0^3}{3V_{Bz}} = 1$. So, from the values obtained for c_1 and c_2, we find that $\frac{\tilde{V}}{V_{Bz}} \approx 0.42$ and $\frac{4\pi p_0^3}{3V_{Bz}} \approx 0.58$. The average gap energy is about $\bar{E} \approx 4$ eV. This yields $\omega_0 \approx 720$ K. This value seems large but not unreasonable. Using the value of a, we can now determine $|\Delta_0| \approx 0.034$. The corresponding values obtained from high temperatures[28] are $\omega_0 \simeq 350$ K and $|\Delta_0| \approx 0.022$.

At high temperatures, $\epsilon \approx c/(T - T_0)$ and $\omega^2(0) \approx A(T - T_0)$. So, $\epsilon \approx cA/\omega^2(0)$. Extrapolating Eq. (13) to high temperatures gives $\epsilon \approx [c_e/\Omega^2(0)]/\omega^2(0)$. According to Ref. 28, $cA = 0.825 \times 10^5 \times 61.6 = 5.1 \times 10^6$. From this work $c_e/\Omega^2(0) = 3.77 \times 10^6$, so the two values are again reasonably close.

Finally, we compare the pressure dependence obtained in this work for $SrTiO_3$ with those obtained for $BaTiO_3$ $KNbO_3$. Within tight binding approximation, the overlap integral can be assumed to vary exponentially with the lattice constant a_0,

$$J = J_0 \exp(-a_0/\lambda). \tag{A15}$$

Under hydrostatic pressure,

$$a_0(p) = a_0(0)(1 - \alpha P), \tag{A16}$$

where $\alpha = S_{11} + 2S_{12}$ is the linear compressibility. In tight binding approximation, using Eqs. (A15) and (A16),

$$\frac{\bar{E}(P) - \bar{E}(0)}{\bar{E}(0)} \simeq \frac{12Ja_0}{\bar{E}\lambda}\alpha P. \tag{A17}$$

In perovskite crystals, $\frac{12J}{\bar{E}}a_0 \simeq 1$ Å, so using Eq. (15), we obtain

$$\gamma = \frac{\alpha}{|\Delta_0|(0)\lambda}. \tag{A18}$$

From Ref. 33 for $ST^{16}O$, $\alpha = 1.82 \times 10^{-4}$ kbar^{-1}, and from this work, $|\Delta_0|(0) = 0.034$ and $\gamma = 0.0262$. This yields $\lambda_{STO} = 0.204$ Å. Similar values were obtained for $BaTiO_3$, $\lambda_{BTO} = 0.1$ Å (Ref. 30) and for $KNbO_3$ $\lambda_{KNO} = 0.3$ Å (Ref. 31).

*yizhak@vms.huji.ac.il

[1] M. Itoh, R. Wang, Y. Inaguma, T. Yamaguchi, Y.-J. Shan, and T. Nakamura, Phys. Rev. Lett. **82**, 3540 (1999).
[2] M. Itoh and R. Wang, Appl. Phys. Lett. **76**, 221 (2000).
[3] Ruiping Wang and Mitsuru Itoh, Phys. Rev. B **62**, R731 (2000).
[4] Ruiping Wang, Norihiko Sakamoto, and Mitsuru Itoh, Phys. Rev. B **62**, R3577 (2000).
[5] R. Wang and M. Itoh, Phys. Rev. B **64**, 174104 (2001).
[6] L. Zhang, W. Kleemann, J. Dec, R. Wang, and M. Itoh, Eur. Phys. J. B **28**, 163 (2002).
[7] E. L. Venturini, G. A. Samara, M. Itoh, and R. Wang, Phys. Rev. B **69**, 184105 (2004).
[8] T. Schneider, H. Beck, and E. Stoll, Phys. Rev. B **13**, 1123 (1976).
[9] R. Morf, T. Schneider, and E. Stoll, Phys. Rev. B **16**, 462 (1977).
[10] H. Taniguchi, T. Yagi, M. Takesada, and M. Itoh, Phys. Rev. B **72**, 064111 (2005).
[11] Takeshi Shigenari, Kohji Abe, Tomohiko Takemoto, Osamu Sanaka, Takashi Akaike, Yoshihide Sakai, Ruiping Wang, and Mitsuru Itoh, Phys. Rev. B **74**, 174121 (2006).
[12] M. Takesada, M. Itoh, and T. Yagi, Phys. Rev. Lett. **96**, 227602 (2006).
[13] Y. Yamada, N. Todoroki, and S. Miyashita, Phys. Rev. B **69**, 024103 (2004). The neutron experimental results are based on the work of Y. Yamada, K. Nomura, and Y. Uesu (unpublished) and of Y. Noda, K. Mochizuki, H. Kimura, Y. Kiomen, R. Wang, and N. Takesue (unpublished).
[14] J. H. Barrett, Phys. Rev. **86**, 118 (1952).
[15] H. Vogt, Phys. Rev. B **51**, 8046 (1995).
[16] A. Bussmann-Holder and A. R. Bishop, Eur. Phys. J. B **53**, 279 (2006).
[17] A. Bussmann-Holder and A. R. Bishop, Europhys. Lett. **76**, 945 (2006).
[18] H. Bilz, G. Benedek, and A. Bussmann-Holder, Phys. Rev. B **35**, 4840 (1987).
[19] A. Bussmann-Holder, H. Bilz, and G. Benedek, Phys. Rev. B **39**, 9214 (1989).
[20] Robert Blinc, Bostjan Zalar, Valentin V. Laguta, and Mitsuru Itoh, Phys. Rev. Lett. **94**, 147601 (2005).
[21] M. Fischer, A Lahmar, M. Maglione, A. San Miguel, J. P. Itie, A. Polian, and F. Baudelet, Phys. Rev. B **49**, 12451 (1994).
[22] Ya. Girshberg and Y. Yacoby, Solid State Commun. **103**, 425 (1997).
[23] Y. Yacoby, Ya. Girshberg, and E. A. Stern, Z. Phys. B: Condens. Matter **104**, 725 (1997).
[24] Ya. Girshberg and Y. Yacoby, J. Phys.: Condens. Matter **11**, 9807 (1999).
[25] Ya. Girshberg and Y. Yacoby, J. Phys.: Condens. Matter **13**, 8817 (2001).
[26] Y. Yacoby, Y. Girshberg, E. A. Stern, and R. Clarke, Phys. Rev. B **74**, 104113 (2006).
[27] K. K. Kobayashi, J. Phys. Soc. Jpn. **24**, 497 (1968).
[28] V. G. Vaks, *Introduction to the Microscopic Theory of Ferroelectricity* (Nauka, Moscow, 1973) (in Russian).
[29] K. A. Müller and H. Burkard, Phys. Rev. B **19**, 3593 (1979).
[30] Y. G. Girshberg, E. V. Bursian, and Y. A. Grushevsky, Ferroelectrics **6**, 53 (1973).
[31] P. Bernasconi, I. Biaggio, M. Zgonik, and P. Gunter, Phys. Rev. Lett. **78**, 106 (1997).
[32] A. A. Abrikosov, L. P. Gorkov, and I. E. Dzyaloshinski, *Methods of Quantum Field Theory in Statistical Physics* (Prentice-Hall, Englewood Cliffs, NJ, 1975).
[33] Hiromoto Uwe and Tunetaro Sakudo, Phys. Rev. B **13**, 271 (1976).